Cite as: E. L. Scheller *et al.*, *Science* 10.1126/science.abo5204 (2022).

Aqueous alteration processes in Jezero crater, Mars—implications for organic geochemistry

Eva L. Scheller[1,2]†*, Joseph Razzell Hollis[3,4]†, Emily L. Cardarelli[3], Andrew Steele[5], Luther W. Beegle[3], Rohit Bhartia[6], Pamela Conrad[5], Kyle Uckert[3], Sunanda Sharma[3], Bethany L. Ehlmann[1,3], William J. Abbey[3], Sanford A. Asher[7], Kathleen C. Benison[8], Eve L. Berger[9,10,11], Olivier Beyssac[12], Benjamin L. Bleefeld[13], Tanja Bosak[2], Adrian J. Brown[14], Aaron S. Burton[11], Sergei V. Bykov[7], Ed Cloutis[15], Alberto G. Fairén[16,17], Lauren DeFlores[3], Kenneth A. Farley[1], Deidra M. Fey[13], Teresa Fornaro[18], Allison C. Fox[11], Marc Fries[11], Keyron Hickman-Lewis[19,20], William F. Hug[6], Joshua E. Huggett[13], Samara Imbeah[13], Ryan S. Jakubek[11], Linda C. Kah[21], Peter Kelemen[22], Megan R. Kennedy[13], Tanya Kizovski[23], Carina Lee[24], Yang Liu[3], Lucia Mandon[25], Francis M. McCubbin[11], Kelsey R. Moore[3], Brian E. Nixon[13], Jorge I. Núñez[26], Carolina Rodriguez Sanchez-Vahamonde[13], Ryan D. Roppel[7], Mitchell Schulte[27], Mark A. Sephton[28], Shiv K. Sharma[29], Sandra Siljeström[30], Svetlana Shkolyar[31,32], David L. Shuster[33], Justin I. Simon[11], Rebecca J. Smith[34], Kathryn M. Stack[3], Kim Steadman[3], Benjamin P. Weiss[2], Alyssa Werynski[13], Amy J. Williams[35], Roger C. Wiens[36,37], Kenneth H. Williford[3,38], Kathrine Winchell[13], Brittan Wogsland[21], Anastasia Yanchilina[39], Rachel Yingling[13], Maria-Paz Zorzano[16]

[1]Division of Geological and Planetary Sciences, California Institute of Technology, Pasadena, CA, USA. [2]Department of Earth, Atmospheric, and Planetary Sciences, Massachusetts Institute of Technology, Cambridge, MA, USA. [3]NASA Jet Propulsion Laboratory, California Institute of Technology, Pasadena, CA, USA. [4]The Natural History Museum, London, UK. [5]Earth and Planets Laboratory, Carnegie Institution for Science, Washington, DC, USA. [6]Photon Systems Incorporated, Covina, CA, USA. [7]Department of Chemistry, University of Pittsburgh, Pittsburgh, PA, USA. [8]Department of Geology and Geography, West Virginia University, Morgantown, WV, USA. [9]Texas State University, San Marcos, TX, USA. [10]Jacobs Johnson Space Center Engineering, Technology and Science Contract, Houston, TX, USA. [11]NASA Johnson Space Center, Houston, TX, USA. [12]Institut de Minéralogie, de Physique des Matériaux et de Cosmochimie, Centre National de la Recherche Scientifique, Sorbonne Université, Muséum National d'Histoire Naturelle, 75005 Paris, France. [13]Malin Space Science Systems, San Diego, CA, USA. [14]Plancus Research, Severna Park, MD, USA. [15]Geography, The University of Winnipeg, Winnipeg, MB, Canada. [16]Centro de Astrobiología, Consejo Superior de Investigaciones Cientificas–Instituto Nacional de Tecnica Aeroespacial, Madrid, Spain. [17]Department of Astronomy, Cornell University, Ithaca, NY, USA. [18]Astrophysical Observatory of Arcetri, Istituto Nazionale di Astrofisica, Florence, Italy. [19]Department of Earth Sciences, The Natural History Museum, London, UK. [20]Dipartimento di Scienze Biologiche, Geologiche e Ambientali, Università di Bologna, Bologna, Italy. [21]Department of Earth and Planetary Sciences, University of Tennessee, Knoxville, TN, USA. [22]Lamont Doherty Earth Observatory, Columbia University, Palisades, NY, USA. [23]Department of Earth Sciences, Brock University, St. Catharines, ON L2S 3A1, Canada. [24]Lunar and Planetary Institute, Universities Space Research Association, Houston, TX, USA. [25]Laboratoire d'Etudes Spatiales et d'Instrumentation en Astrophysique, Observatoire de Paris, Centre National de la Recherche Scientifique, Sorbonne Université, Université Paris Diderot, 92195 Meudon, France. [26]Johns Hopkins University Applied Physics Laboratory, Laurel, MD, USA. [27]Mars Exploration Program, NASA Headquarters, Washington, DC, USA. [28]Earth Science and Engineering, South Kensington Campus, Imperial College London, SW7 2AZ London, UK. [29]Hawaii Institute of Geophysics and Planetology, University of Hawaii at Manoa, Honolulu, HI, USA. [30]Research Institutes of Sweden, Stockholm, Sweden. [31]Department of Astronomy, University of Maryland, College Park, MD, USA. [32]NASA Goddard Space Flight Center, Greenbelt, MD, USA. [33]Earth and Planetary Science, University of California Berkeley, Berkeley, CA, USA. [34]Department of Geosciences, Stony Brook University, Stony Brook, NY, USA. [35]Department of Geological Sciences, University of Florida, Gainesville, FL, USA. [36]Los Alamos National Laboratory, Los Alamos, NM, USA. [37]Earth, Atmospheric, and Planetary Sciences, Purdue University, West Lafayette, IN, USA. [38]Blue Marble Space Institute of Science, Seattle, WA, USA. [39]Impossible Sensing, St. Louis, MO, USA.

†These authors contributed equally to this work.

***Corresponding author. Email: eschelle@mit.edu**

The Perseverance rover landed in Jezero crater, Mars in February 2021. We used the Scanning Habitable Environments with Raman and Luminescence for Organics and Chemicals (SHERLOC) instrument to perform deep ultraviolet Raman and fluorescence spectroscopy of three rocks within the crater. We identify evidence for two distinct ancient aqueous environments at different times. Reactions with liquid water formed carbonates in an olivine-rich igneous rock. A sulfate-perchlorate mixture is present in the rocks, probably formed by later modifications of the rocks by brine. Fluorescence signatures consistent with aromatic organic compounds occur throughout these rocks, preserved in minerals related to both aqueous environments.

The Perseverance rover landed in Jezero crater, Mars to investigate the geology of the crater, identify habitable environments, assess whether life ever existed on Mars, and to collect samples for potential return to Earth (*1*). Jezero hosted an open-basin lake during the Noachian era (~3.7 Ga) (*1*, *2*), contains geologic units associated with the largest carbonate deposit identified on Mars (*2*–*4*), and contains a well-preserved delta with clay and carbonate-bearing sediments, which might contain organics (*1*). Organics have previously been detected on Mars (*5*, *6*).

We investigated the spatial and mineralogical context of organics in Jezero crater using the rover's SHERLOC instrument (Scanning Habitable Environments with Raman and Luminescence for Organics and Chemicals), a deep-ultraviolet fluorescence and Raman spectrometer capable of mapping organic and mineral composition with a spatial resolution of 100 μm (*7*). Complementary elemental chemistry analyses were performed using the PIXL (Planetary Instrument for X-ray Lithochemistry) (*8–11*) and SuperCam instruments (*9*).

We identify organics and aqueously formed minerals at Jezero crater in three rock targets (*8*) analyzed during the first 208 Martian days of the mission (Fig. 1) located in two different geological units within the floor of Jezero crater (*9*, *12*). The Garde target is from the altered ultramafic Séítah Formation (Fm), orbitally mapped as the Crater Floor Fractured 1 unit (CF-f1) (Fig. 1) (*9*, *12*). The Guillaumes and Bellegarde targets are from the overlying and therefore younger basaltic Máaz Fm, orbitally mapped as the ~2.3-2.6 Ga (*13*) Crater Floor Fractured Rough unit (CF-fr) (*9*, *12*). The Perseverance rover drilled four rock samples from the Séítah Fm. Two drilled rock samples were obtained from the Bellegarde rock, while the Guillaumes drilled rock sample attempt, Roubion, failed (*12*). These six rock samples are planned to be returned to Earth.

All three Raman spectral scans (*8*) from Garde exhibit strong peaks at Raman shifts between 1080 and 1090 cm^{-1} (investigated in 38 separate scan points) attributed to carbonate [spectrum 1 and region of interest (ROI) 1-4 in Fig. 2H], and peaks with a peak position range of 820 to 840 cm^{-1} (n=60) attributed to olivine (ROI 1 and 4 in Fig. 2H) (*8*, *13*, *14*). Olivines were found to be more Fe-rich than laboratory measured olivines with fosterite numbers [defined as $Mg/(Mg + Fe^{2+}) \times 100$] of 80-90 (*13*), while carbonates are likely mixed Fe- and Mg-species based on 1080-1087 cm^{-1} peak positions (*8*), and Ca-dominated species are excluded based on PIXL data (*11*). These spectral detections were overlaid on Wide-Angle Topographic Sensor for Operations and eNgineering (WATSON) camera images to compare spectral positions with textures (*8*). Olivine and carbonate are associated with μm- to mm-sized light-toned tan, reddish-brown, and dark-toned sub-angular grains as well as light-toned intergranular spaces (Fig. 2, B and E). Spectral features of olivines and carbonates often co-occur in a single spectrum; however, there are also areas where either olivine or carbonate occur independently. Spectral observations of a weak, broad Raman peak centered ~1060 cm^{-1} (FWHM ~200 cm^{-1}) could indicate a disordered phase consistent with amorphous silicates, which is often difficult to detect given the low band intensity (Fig. 2). A peak at 960 ± 5 cm^{-1} is likely phosphate, although perchlorates cannot be excluded (Fig. 2).

Garde detail scans (*8*) exhibit strong fluorescence signatures, centered at ~340 nm, that spatially correlate with carbonate, probable phosphate, and amorphous silicate spectra localized within narrow intergranular spaces (Fig. 2, E and F). A less intense fluorescence band centered at 285 nm typically accompanies the 340 nm fluorescence. Other areas exhibit no fluorescence (Fig. 2C).

Guillaumes features white and reddish brown patches, 1-2 mm across, that do not have well-formed crystal faces (Fig. 3A and fig. S1). These are secondary materials within a basaltic igneous rock (*9*), which we interpret as void fills, that correlate with sulfate and perchlorate spectra. Spectra with high intensity 950-955 cm^{-1} peaks and minor 1090-1095 cm^{-1} and 1150-1155 cm^{-1} peaks match laboratory measurements of anhydrous Na-perchlorate (*8*) (Fig. 3G and fig. S4). Two strong Na-perchlorate detections correlate with centers of the brightest material within the anhedral patches (*8*). Guillaumes spectra commonly contain a single low-intensity peak positioned at 950-955 cm^{-1}. We interpret these as low intensity Na-perchlorate peaks, although the cation species is uncertain due to a lack of resolvable minor peaks (*8*) (Fig. 3G). Other spectra exhibit both 950-955 cm^{-1} peaks and equally strong 1010-1020 cm^{-1} peaks, with low intensity broad features at 1120 ± 5 cm^{-1}, and occasional broad 3450 ± 5 cm^{-1} hydration features, consistent with a mixture of sulfate and perchlorate that is minimally hydrated (Fig. 3G). A Ca-sulfate species best explains these spectra when coupled with elemental chemistry data from PIXL and SuperCam (*8*). Two detected 965 cm^{-1} peaks are likely phosphates, although perchlorates cannot be excluded.

Bellegarde contains white 0.5-1 mm secondary crystals with well-formed and sharp crystal faces and reddish brown semi-isopachous rims (*8*) (fig. S2). We interpret these as void fills within a basaltic igneous rock. These crystals exhibit 1010-1020 cm^{-1} peaks, similarly attributed to Ca-sulfate when coupled with elemental chemistry data (*8*). Several of the sulfate peaks are also associated with a narrow low-intensity hydration feature at 3560 ± 5 cm^{-1}, consistent with hydrated Ca-sulfates (fig. S3). The Bellegarde target contains a single 1080 ± 5 cm^{-1} peak of possible Ca-carbonate (Fig. 4 and fig. S2). Narrow peaks at 975 cm^{-1} peak could not definitively be identified and could be phosphate or perchlorate (*8*). The SHERLOC mineral detections within the Bellegarde and Guillaumes targets are consistent with the results from other Perseverance instruments (*8*, *9*, *11*) (figs. S5 and S6).

Guillaumes and Bellegarde targets commonly exhibit a weak, broad fluorescence feature with a maximum at ~340 nm (Figs. 3D and 4D) that appears to be widely distributed across each surface and is occasionally correlated with reddish-brown materials. Although this feature sometimes co-occurs with perchlorate, sulfate, and possibly phosphate, it occurs equally often in areas with unidentified mineralogy. Bellegarde has two other signatures at ~275 and ~305 nm

(Fig. 4D), which are strong and localized on specific, light-toned features. The ~305 nm signature is associated with detected sulfate (Fig. 4, D to F, and fig. S2). In Guillaumes, a second fluorescence signature at ~275 nm (Fig. 3D) is observed in two locations, approximately 300 μm in diameter, coincident with previous SuperCam laser spots (*8*).

Observation of olivine and carbonate mixtures within the Garde target of the Séítah Fm is consistent with orbital infrared observations (*2–4*) and substantiated by multiple lines of evidence (*9–11*). Previously proposed hypotheses for the precipitation of these carbonates include low-temperature and high-temperature aqueous alteration of olivine-rich igneous materials, which we will subsequently refer to as ultramafic protolith (*3*, *15–17*), or precipitation from lake or groundwater (*4*, *15–17*). Our 10-100 μm-scale textural and spectroscopic evidence supports carbonate formation through aqueous alteration of an ultramafic protolith, known as carbonation. The supporting evidence includes: (i) Carbonate cation compositions consistent with those of olivines, suggesting mixed Fe- and Mg-olivine gave rise to mixed Fe- and Mg-carbonates, similar to on Earth and within Martian meteorites (*16*, *18*, *19*). (ii) The observed carbonates co-occur with hydrated materials (*9*) and potentially aqueously formed amorphous silicates and phosphate. (iii) The spectral and textural variation of olivine and carbonate dominated zones within both primary grains and intergranular spaces are expected for carbonated ultramafic protoliths on Earth (*16*) and within Martian meteorites (*18*, *19*).

These observations suggest that the degree of aqueous alteration to the ultramafic protolith was not pervasive, because large olivine-rich domains remain intact. In contrast, the alteration of the primary lithology is pervasive and occurs throughout (not in specific spatial domains e.g., fractures). In ultramafic alteration environments on Earth (*16*) and in Martian meteorites (*18*, *19*), carbonation can be associated with the formation of oxides, hydroxides, and/or Fe/Mg-rich phyllosilicates, which have not been observed (*9*). Carbonation can occur in a wide range of temperatures from low to ambient to hydrothermal/metamorphic (*15–17*). Other alteration minerals, such as serpentine, have not been definitively observed in the Séitah Fm to date, which could suggest time limited interactions, low water rock ratios, or ambient fluid temperatures during carbonation (*3*, *15–17*).

The similarity between the mineralogy of the Garde target in the Séítah Fm to the surrounding widespread, regional olivine-carbonate-bearing unit with a similar orbital spectroscopic signature and geomorphological texture (*3*, *4*, *15*, *16*) suggests that carbonation of olivine may have occurred throughout this extensive region on ancient Mars (~2.7-3.8 Ga). These observations parallel those made by the Spirit rover in Gusev Crater (*20*) and within (1.3-4 Ga) Martian meteorites (*18*, *19*). Modeling has suggested that carbonate deposition could have played a role in the evolution of Mars' atmosphere (*3*, *17*, *21*), but the geological nature of such a depositional mechanism had remained unexplained. Taken together, micron-scale SHERLOC observations of this phenomenon complements previous orbital and meteorite observations and demonstrates alteration of igneous materials resulting in geological deposition of carbonates.

Jezero crater perchlorate detections, like those found by the Phoenix lander (*22*), have been substantiated using three independent instruments (*9*). Previous evidence for Martian perchlorates includes observations by the Curiosity rover (*23*), proposed but later disputed orbital detections (*24*), and detection within the Tissint meteorite (*25*). The SHERLOC perchlorate detections differ from previous mission observations because they are observed within the interior of a rock and not on the surface, are related to aqueous processes, and are likely Na-perchlorate [not previously detected Ca-, Fe- or Mg-perchlorates (*23*)].

Previous hypotheses for perchlorate formation on Mars are (i) irradiation of chlorine-bearing parent minerals (*26*), (ii) atmospheric oxidation of chlorine species (*27*), or (iii) formation from brines (*25*). Perchlorates could also be mobilized in thin films of fluid (*23*). The Jezero perchlorates form white void-fills within rock interiors, and did not form directly on the surface as expected from materials formed by cosmic irradiation or atmospheric oxidation, indicating either formation or mobilization through briny fluids after basalt formation. The concomitant detection of sulfates and perchlorates within the Guillaumes target suggests that sulfate formed together with perchlorate or parent chlorine-bearing species, such as halite, within percolating briny waters that were then subsequently oxidized to perchlorate. Bellegarde exhibited sulfate without perchlorate, suggesting these brines did not precipitate chlorine-bearing parent species, that perchlorate formation was not pervasive, or that perchlorates were since dissolved. Perchlorates are easily dissolved, and therefore perchlorates likely formed when these rocks were last exposed to liquid water. Perchlorate and sulfate detections within the stratigraphically younger Máaz Fm (*9*) substantiates an aqueous environment on Mars that occurred separately from the stratigraphically older (*9*) Séítah Fm carbonation environment.

Deep ultraviolet (DUV) fluorescence is particularly sensitive to aromatic organic compounds, and the fluorescence signatures observed in all three targets are consistent with emission from aromatic organic compounds containing 1 or 2 fused aromatic rings and/or aromatic heterocycles (*7*, *8*, *28*) (fig. S7). Although fluorescence signatures cannot be assigned to specific organic compounds, the ~340 nm fluorescence is consistent with a base structure of 2-ring aromatic organics like naphthalene, whereas ~275-285 nm fluorescence is more consistent with 1-ring aromatic organics like benzene (*8*, *28*).

The ~305 nm fluorescence could indicate either 1- or 2-ring aromatics, depending on functional groups. We interpret ~305 nm and ~275 nm fluorescence as organics that occurred with sulfates within the Bellegarde target (Fig. 4, D to F), while we interpret ~285 nm fluorescence as organics that occurred with carbonate-phosphate-amorphous silicate brown microcrystalline alteration zones within the Garde target (Fig. 2) (*8*). The ~340 nm fluorescence co-occurs with carbonate-phosphate-amorphous silicate alteration zones in Garde but is not associated with particular phases in Guillaumes and Bellegarde (*8*). This phosphate-correlated 340 nm fluorescence could be explained by organics in the same alteration zone, and/or a minor component of fluorescent cerium present within the phosphate (*8*). In Guillaumes and Bellegarde, 340 nm fluorescence is predominantly uncoupled from phosphate detections, suggesting part of this signal is best assigned to organics (*8*). However, that some or all of the ~340 nm fluorescence signal is from cerium cannot be excluded (*8*).

When combined with Curiosity observations of organic material in mudstones (*29*), the presence of organic material in igneous rocks implies a diverse relationship between geological processes and organic compounds on Mars. Several explanations for the presence of Martian organics are possible, e.g., infall of meteoritic material (*6*), in situ synthesis mechanisms (*18*, *19*, *25*), or a putative relic Martian biosphere. The association between organics and sulfate-, phosphate-, perchlorate-, carbonate-, and amorphous silicate-bearing mineralogy, as well as alteration textures, suggests that aqueous alteration of igneous rocks could have played a role in the preservation (or synthesis) of these organics, as seen for similar organics-mineral correlations in Martian meteorites (*18*, *19*, *25*). However, potentially organic, widespread ~340 nm fluorescence could suggest other processes, such as dust, contributed to detections. Some mineral phase associations might not be apparent due to instrumental limitations (*8*).

We did not detect Raman peaks consistent with aromatic organic compounds, such as the C=C stretching mode (or G band) around ~1600 cm^{-1}. However, Raman scattered light is several orders of magnitude weaker than fluorescence (*8*, *28*). Organic concentrations were likely insufficient to produce detectable Raman scattering, either due to low original concentration or subsequent degradation. We estimate a range from 5×10^{-11} to 3×10^{-10} grams of aromatic organics in localized scan points that encompass an estimated 6×10^{-7} grams of rock (*8*). Estimates from the average fluorescence maps suggest a bulk concentration of 0.1 to 10 ppm, with higher concentrations associated with more aqueously altered surfaces (*8*), consistent with known bulk concentrations of organics, containing one and two ring aromatic species, indigenous to Martian meteorites [11.2 ± 6.9 ppm (*18*)] and Curiosity rover detections in mudstones [~70 ppbw to 10.6 ± 8.9 ppm (*6*, *29*)].

Collectively, the data show the drilled samples collected by Perseverance from the floor of Jezero crater are likely to contain evidence for carbonation and formation of sulfates and perchlorates. Fluorescence signatures consistent with organics present within these materials indicates an interplay between igneous rocks, aqueous alteration, and organic material on Mars.

REFERENCES AND NOTES

1. K. A. Farley, K. H. Williford, K. M. Stack, R. Bhartia, A. Chen, M. de la Torre, K. Hand, Y. Goreva, C. D. K. Herd, R. Hueso, Y. Liu, J. N. Maki, G. Martinez, R. C. Moeller, A. Nelessen, C. E. Newman, D. Nunes, A. Ponce, N. Spanovich, P. A. Willis, L. W. Beegle, J. F. Bell III, A. J. Brown, S.-E. Hamran, J. A. Hurowitz, S. Maurice, D. A. Paige, J. A. Rodriguez-Manfredi, M. Schulte, R. C. Wiens, Mars 2020 mission overview. *Space Sci. Rev.* **216**, 142 (2020). doi:10.1007/s11214-020-00762-y
2. T. A. Goudge, J. F. Mustard, J. W. Head, C. I. Fassett, S. M. Wiseman, Assessing the mineralogy of the watershed and fan deposits of the Jezero crater paleolake system, Mars. *J. Geophys. Res. Planets* **120**, 775–808 (2015). doi:10.1002/2014JE004782
3. B. L. Ehlmann, J. F. Mustard, S. L. Murchie, F. Poulet, J. L. Bishop, A. J. Brown, W. M. Calvin, R. N. Clark, D. J. D. Marais, R. E. Milliken, L. H. Roach, T. L. Roush, G. A. Swayze, J. J. Wray, Orbital identification of carbonate-bearing rocks on Mars. *Science* **322**, 1828–1832 (2008). doi:10.1126/science.1164759 Medline
4. B. H. Horgan, R. B. Anderson, G. Dromart, E. S. Amador, M. S. Rice, The mineral diversity of Jezero crater: Evidence for possible lacustrine carbonates on Mars. *Icarus* **339**, 113526 (2020). doi:10.1016/j.icarus.2019.113526
5. R. Navarro-González, E. Vargas, J. de la Rosa, A. C. Raga, C. P. McKay, Reanalysis of the Viking results suggests perchlorate and organics at midlatitudes on Mars. *J. Geophys. Res. Planets* **115**, E12010 (2010). doi:10.1029/2010JE003599
6. J. L. Eigenbrode, R. E. Summons, A. Steele, C. Freissinet, M. Millan, R. Navarro-González, B. Sutter, A. C. McAdam, H. B. Franz, D. P. Glavin, P. D. Archer Jr., P. R. Mahaffy, P. G. Conrad, J. A. Hurowitz, J. P. Grotzinger, S. Gupta, D. W. Ming, D. Y. Sumner, C. Szopa, C. Malespin, A. Buch, P. Coll, Organic matter preserved in 3-billion-year-old mudstones at Gale crater, Mars. *Science* **360**, 1096–1101 (2018). doi:10.1126/science.aas9185 Medline
7. R. Bhartia, L. W. Beegle, L. DeFlores, W. Abbey, J. Razzell Hollis, K. Uckert, B. Monacelli, K. S. Edgett, M. R. Kennedy, M. Sylvia, D. Aldrich, M. Anderson, S. A. Asher, Z. Bailey, K. Boyd, A. S. Burton, M. Caffrey, M. J. Calaway, R. Calvet, B. Cameron, M. A. Caplinger, B. L. Carrier, N. Chen, A. Chen, M. J. Clark, S. Clegg, P. G. Conrad, M. Cooper, K. N. Davis, B. Ehlmann, L. Facto, M. D. Fries, D. H. Garrison, D. Gasway, F. T. Ghaemi, T. G. Graff, K. P. Hand, C. Harris, J. D. Hein, N. Heinz, H. Herzog, E. Hochberg, A. Houck, W. F. Hug, E. H. Jensen, L. C. Kah, J. Kennedy, R. Krylo, J. Lam, M. Lindeman, J. McGlown, J. Michel, E. Miller, Z. Mills, M. E. Minitti, F. Mok, J. Moore, K. H. Nealson, A. Nelson, R. Newell, B. E. Nixon, D. A. Nordman, D. Nuding, S. Orellana, M. Pauken, G. Peterson, R. Pollock, H. Quinn, C. Quinto, M. A. Ravine, R. D. Reid, J. Riendeau, A. J. Ross, J. Sackos, J. A. Schaffner, M. Schwochert, M. O Shelton, R. Simon, C. L. Smith, P. Sobron, K. Steadman, A. Steele, D. Thiessen, V. D. Tran, T. Tsai, M. Tuite, E. Tung, R. Wehbe, R. Weinberg, R. H. Weiner, R. C. Wiens, K. Williford, C. Wollonciej, Y.-H. Wu, R. A. Yingst, J. Zan, Perseverance's Scanning Habitable Environments with Raman and Luminescence for Organics and Chemicals (SHERLOC) Investigation. *Space Sci. Rev.* **217**, 58 (2021). doi:10.1007/s11214-021-00812-z
8. Materials and methods are available as supplementary materials.
9. K. A. Farley, K. M. Stack, D. L. Shuster, B. H. N. Horgan, J. A. Hurowitz, J. D. Tarnas, J. I. Simon, V. Z. Sun, E. L. Scheller, K. R. Moore, S. M. McLennan, P. M. Vasconcelos, R. C. Wiens, A. H. Treiman, L. E. Mayhew, O. Beyssac, T. V. Kizovski, N. J. Tosca, K. H. Williford, L. S. Crumpler, L. W. Beegle, J. F. Bell III, B. L. Ehlmann, Y. Liu, J. N. Maki, M. E. Schmidt, A. C. Allwood, H. E. F. Amundsen, R. Bhartia, T. Bosak, A. J. Brown, B. C. Clark, A. Cousin, O. Forni, T. S. J. Gabriel, Y. Goreva, S. Gupta, S.-E. Hamran, C. D. K. Herd, K. Hickman-Lewis, J. R. Johnson, L. C. Kah, P. B. Kelemen, K. B. Kinch, L. Mandon, N. Mangold, C. Quantin-Nataf, M. S. Rice, P. S. Russell, S. Sharma, S. Siljeström, A. Steele, R. Sullivan, M. Wadhwa, B. P. Weiss, A. J. Williams, B. V. Wogsland, P. A. Willis, T. A. Acosta-Maeda, P. Beck, K.

Benzerara, S. Bernard, A. S. Burton, E. L. Cardarelli, B. Chide, E. Clavé, E. A. Cloutis, B. A. Cohen, A. D. Czaja, V. Debaille, E. Dehouck, A. G. Fairén, D. T. Flannery, S. Z. Fleron, T. Fouchet, J. Frydenvang, B. J. Garczynski, E. F. Gibbons, E. M. Hausrath, A. G. Hayes, J. Henneke, J. L. Jørgensen, E. M. Kelly, J. Lasue, S. Le Mouélic, J. M. Madariaga, S. Maurice, M. Merusi, P.-Y. Meslin, S. M. Milkovich, C. C. Million, R. C. Moeller, J. I. Núñez, A. M. Ollila, G. Paar, D. A. Paige, D. A. K. Pedersen, P. Pilleri, C. Pilorget, P. C. Pinet, J. W. Rice Jr., C. Royer, V. Sautter, M. Schulte, M. A. Sephton, S. K. Sharma, S. F. Sholes, N. Spanovich, M. St. Clair, C. D. Tate, K. Uckert, S. J. VanBommel, A. G. Yanchilina, M.-P. Zorzano, Aqueously altered igneous rocks sampled on the floor of Jezero crater, Mars. *Science* **377**, eabo2196 (2022). doi:10.1126/science.abo2196 Medline

10. Y. Liu, M. M. Tice, M. E. Schmidt, A. H. Treiman, T. V. Kizovski, J. A. Hurowitz, A. C. Allwood, J. Henneke, D. A. K. Pedersen, S. J. VanBommel, M. W. M. Jones, A. L. Knight, B. J. Orenstein, B. C. Clark, W. T. Elam, C. M. Heirwegh, T. Barber, L. W. Beegle, K. Benzerara, S. Bernard, O. Beyssac, T. Bosak, A. J. Brown, E. L. Cardarelli, D. C. Catling, J. R. Christian, E. A. Cloutis, B. A. Cohen, S. Davidoff, A. G. Fairén, K. A. Farley, D. T. Flannery, A. Galvin, J. P. Grotzinger, S. Gupta, J. Hall, C. D. K. Herd, K. Hickman-Lewis, R. P. Hodyss, B. H. N. Horgan, J. R. Johnson, J. L. Jørgensen, L. C. Kah, J. N. Maki, L. Mandon, N. Mangold, F. M. McCubbin, S. M. McLennan, K. Moore, M. Nachon, P. Nemere, L. D. Nothdurft, J. I. Núñez, L. O'Neil, C. M. Quantin-Nataf, V. Sautter, D. L. Shuster, K. L. Siebach, J. I. Simon, K. P. Sinclair, K. M. Stack, A. Steele, J. D. Tarnas, N. J. Tosca, K. Uckert, A. Udry, L. A. Wade, B. P. Weiss, R. C. Wiens, K. H. Williford, M.-P. Zorzano, An olivine cumulate outcrop on the floor of Jezero crater, Mars. *Science* **377**, 1513–1519 (2022). doi:10.1126/science.abo2756 Medline
11. M. M. Tice, J. A. Hurowitz, A. C. Allwood, M. W. M. Jones, B. J. Orenstein, S. Davidoff, A. P. Wright, D. A. K. Pedersen, J. Henneke, N. J. Tosca, K. R. Moore, B. C. Clark, S. M. McLennan, D. T. Flannery, A. Steele, A. J. Brown, M.-P. Zorzano, K. Hickman-Lewis, Y. Liu, S. J. VanBommel, M. E. Schmidt, T. V. Kizovski, A. H. Treiman, L. O'Neil, A. G. Fairén, D. L. Shuster, S. Gupta, PIXL Team, Alteration history of Séítah formation rocks inferred by PIXL x-ray fluorescence, x-ray diffraction, and multispectral imaging on Mars. *Sci. Adv.* 10.1126/sciadv.abp9084 (2022). doi:10.1126/sciadv.abp9084
12. K. M. Stack, N. R. Williams, F. Calef III, V. Z. Sun, K. H. Williford, K. A. Farley, S. Eide, D. Flannery, C. Hughes, S. R. Jacob, L. C. Kah, F. Meyen, A. Molina, C. Q. Nataf, M. Rice, P. Russell, E. Scheller, C. H. Seeger, W. J. Abbey, J. B. Adler, H. Amundsen, R. B. Anderson, S. M. Angel, G. Arana, J. Atkins, M. Barrington, T. Berger, R. Borden, B. Boring, A. Brown, B. L. Carrier, P. Conrad, H. Dypvik, S. A. Fagents, Z. E. Gallegos, B. Garczynski, K. Golder, F. Gomez, Y. Goreva, S. Gupta, S.-E. Hamran, T. Hicks, E. D. Hinterman, B. N. Horgan, J. Hurowitz, J. R. Johnson, J. Lasue, R. E. Kronyak, Y. Liu, J. M. Madariaga, N. Mangold, J. McClean, N. Miklusicak, D. Nunes, C. Rojas, K. Runyon, N. Schmitz, N. Scudder, E. Shaver, J. SooHoo, R. Spaulding, E. Stanish, L. K. Tamppari, M. M. Tice, N. Turenne, P. A. Willis, R. A. Yingst, Photogeologic map of the perseverance rover field site in Jezero Crater constructed by the Mars 2020 Science Team. *Space Sci. Rev.* **216**, 127 (2020). doi:10.1007/s11214-020-00739-x Medline
13. J. Razzell Hollis, W. Abbey, L. W. Beegle, R. Bhartia, B. L. Ehlmann, J. Miura, B. Monacelli, K. Moore, A. Nordman, E. Scheller, K. Uckert, Y.-H. Wu, A deep-ultraviolet Raman and Fluorescence spectral library of 62 minerals for the SHERLOC instrument onboard Mars 2020. *Planet. Space Sci.* **209**, 105356 (2021). doi:10.1016/j.pss.2021.105356
14. J. Razzell Hollis, S. Ireland, W. Abbey, R. Bhartia, L. W. Beegle, Deep-ultraviolet Raman spectra of Mars-relevant evaporite minerals under 248.6 nm excitation. *Icarus* **357**, 114067 (2021). doi:10.1016/j.icarus.2020.114067
15. J. D. Tarnas, K. M. Stack, M. Parente, A. H. D. Koeppel, J. F. Mustard, K. R. Moore, B. H. N. Horgan, F. P. Seelos, E. A. Cloutis, P. B. Kelemen, D. Flannery, A. J. Brown, K. R. Frizzell, P. Pinet, Characteristics, origins, and biosignature preservation potential of carbonate-bearing rocks within and outside of Jezero crater. *J. Geophys. Res. Planets* **126**, JE006898 (2021). Medline
16. E. L. Scheller, C. Swindle, J. Grotzinger, H. Barnhart, S. Bhattacharjee, B. L. Ehlmann, K. Farley, W. W. Fischer, R. Greenberger, M. Ingalls, P. E. Martin, D. Osorio-Rodriguez, B. P. Smith, Formation of magnesium carbonates on Earth and implications for Mars. *J. Geophys. Res. Planets* **126**, JE006828 (2021). Medline
17. V. F. Chevrier, M. Morisson, Carbonate-phyllosilicate parageneses and environments of aqueous alteration in Nili Fossae and Mars. *J. Geophys. Res. Planets* **126**, e2020JE006698 (2021). doi:10.1029/2020JE006698
18. A. Steele, F. M. McCubbin, M. D. Fries, The provenance, formation, and implications of reduced carbon phases in Martian meteorites. *Meteorit. Planet. Sci.* **51**, 2203–2225 (2016). doi:10.1111/maps.12670
19. A. Steele, L. G. Benning, R. Wirth, A. Schreiber, T. Araki, F. M. McCubbin, M. D. Fries, L. R. Nittler, J. Wang, L. J. Hallis, P. G. Conrad, C. Conley, S. Vitale, A. C. O'Brien, V. Riggi, K. Rogers, Organic synthesis associated with serpentinization and carbonation on early Mars. *Science* **375**, 172–177 (2022). doi:10.1126/science.abg7905 Medline
20. R. V. Morris, S. W. Ruff, R. Gellert, D. W. Ming, R. E. Arvidson, B. C. Clark, D. C. Golden, K. Siebach, G. Klingelhöfer, C. Schröder, I. Fleischer, A. S. Yen, S. W. Squyres, Identification of carbonate-rich outcrops on Mars by the Spirit rover. *Science* **329**, 421–424 (2010). doi:10.1126/science.1189667 Medline
21. R. Hu, D. M. Kass, B. L. Ehlmann, Y. L. Yung, Tracing the fate of carbon and the atmospheric evolution of Mars. *Nat. Commun.* **6**, 10003 (2015). doi:10.1038/ncomms10003 Medline
22. M. H. Hecht, S. P. Kounaves, R. C. Quinn, S. J. West, S. M. M. Young, D. W. Ming, D. C. Catling, B. C. Clark, W. V. Boynton, J. Hoffman, L. P. Deflores, K. Gospodinova, J. Kapit, P. H. Smith, Detection of perchlorate and the soluble chemistry of martian soil at the Phoenix lander site. *Science* **325**, 64–67 (2009). doi:10.1126/science.1172466 Medline
23. P. E. Martin, K. A. Farley, P. D. Archer Jr., J. V. Hogancamp, K. L. Siebach, J. P. Grotzinger, S. M. McLennan, Reevaluation of perchlorate in Gale crater rocks suggests geologically recent perchlorate addition. *J. Geophys. Res. Planets* **125**, e2019JE006156 (2020). doi:10.1029/2019JE006156
24. E. K. Leask, B. L. Ehlmann, M. M. Dundar, S. L. Murchie, F. P. Seelos, Challenges in the search for perchlorate and other hydrated minerals with 2.1-μm absorptions on Mars. *Geophys. Res. Lett.* **45**, 12180–12189 (2018). doi:10.1029/2018GL080077 Medline
25. A. Steele, L. G. Benning, R. Wirth, S. Siljeström, M. D. Fries, E. Hauri, P. G. Conrad, K. Rogers, J. Eigenbrode, A. Schreiber, A. Needham, J. H. Wang, F. M. McCubbin, D. Kilcoyne, J. D. Rodriguez Blanco, Organic synthesis on Mars by electrochemical reduction of CO_2. *Sci. Adv.* **4**, eaat5118 (2018). doi:10.1126/sciadv.aat5118 Medline
26. B. L. Carrier, S. P. Kounaves, The origins of perchlorate in the Martian soil. *Geophys. Res. Lett.* **42**, 3739–3745 (2015). doi:10.1002/2015GL064290
27. D. C. Catling, M. W. Claire, K. J. Zahnle, R. C. Quinn, B. C. Clark, M. H. Hecht, S. Kounaves, Atmospheric origins of perchlorate on Mars and in the Atacama. *J. Geophys. Res. Planets* **115**, E1 (2010). doi:10.1029/2009JE003425
28. R. Bhartia, W. F. Hug, E. C. Salas, R. D. Reid, K. K. Sijapati, A. Tsapin, W. Abbey, K. H. Nealson, A. L. Lane, P. G. Conrad, Classification of organic and biological materials with deep ultraviolet excitation. *Appl. Spectrosc.* **62**, 1070–1077 (2008). doi:10.1366/000370208786049123 Medline
29. C. Freissinet, D. P. Glavin, P. R. Mahaffy, K. E. Miller, J. L. Eigenbrode, R. E. Summons, A. E. Brunner, A. Buch, C. Szopa, P. D. Archer Jr., H. B. Franz, S. K. Atreya, W. B. Brinckerhoff, M. Cabane, P. Coll, P. G. Conrad, D. J. Des Marais, J. P. Dworkin, A. G. Fairén, P. François, J. P. Grotzinger, S. Kashyap, I. L. Ten Kate, L. A. Leshin, C. A. Malespin, M. G. Martin, F. J. Martin-Torres, A. C. McAdam, D. W. Ming, R. Navarro-González, A. A. Pavlov, B. D. Prats, S. W. Squyres, A. Steele, J. C. Stern, D. Y. Sumner, B. Sutter, M.-P. Zorzano, Organic molecules in the Sheepbed Mudstone, Gale Crater, Mars. *J. Geophys. Res. Planets* **120**, 495–514 (2015). doi:10.1002/2014JE004737 Medline
30. USGS Astrogeology Science Center, Mars 2020 terrain relative navigation HiRISE orthorectified image mosaic, Astropedia (2020); https://doi.org/10.5066/P9QJDP48.
31. L. W. Beegle, R. Bhartia, Mars 2020 SHERLOC Bundle, Planetary Data System (2021); https://doi.org/10.17189/1522643.
32. J. F. Bell, J. N. Maki, Mars 2020 Mast Camera Zoom Data Bundle, from Operations Team, calibrated products, Planetary Data System (2021); https://doi.org/10.17189/bs6b-4782.
33. J. N. Maki, Mars 2020 Engineering Camera (ECAM) Bundles, Planetary Data System (2021); https://doi.org/10.17189/1522847.
34. A. C. Allwood, J. A. Hurowitz, Mars 2020 PIXL Raw and Processed Data Bundle, Planetary Data System (2021); https://doi.org/10.17189/1522645.
35. R. C. Wiens, M. A. Sylvestre, Mars 2020 SuperCam Bundle, Planetary Data System

(2021); https://doi.org/10.17189/1522646.
36. K. Uckert, LoupeV5.1.5, Zenodo (2022); https://doi.org/10.5281/zenodo.7062998.
37. E. L. Scheller, Laboratory datasets - Raman spectra, Zenodo (2022); https://doi.org/10.5281/zenodo.7212486.
38. M. D. Fries, C. Lee, R. Bhartia, J. Razzell Hollis, L. W. Beegle, K. Uckert, T. G. Graff, W. Abbey, Z. Bailey, E. L. Berger, A. S. Burton, M. J. Callaway, E. L. Cardarelli, K. N. Davis, L. DeFlores, K. S. Edgett, A. C. Fox, D. H. Garrison, N. C. Haney, R. S. Harrington, R. S. Jakubek, M. R. Kennedy, K. Hickman-Lewis, F. M. McCubbin, E. Miller, B. Monacelli, R. Pollock, R. Rhodes, S. Siljeström, S. Sharma, C. L. Smith, A. Steele, M. Sylvia, V. D. Tran, R. H. Weiner, A. G. Yanchilina, R. Aileen Yingst, The SHERLOC calibration target on the Mars 2020 Perseverance rover: Design, operations, outreach, and future human exploration functions. *Space Sci. Rev.* **218**, 218 (2022). doi:10.1007/s11214-022-00907-1
39. K. Uckert, R. Bhartia, J. Michel, A semi-autonomous method to detect cosmic rays in Raman hyperspectral data sets. *Appl. Spectrosc.* **73**, 1019–1027 (2019). doi:10.1177/0003702819850584 Medline
40. M. Newville, T. Stensitzki, D. B. Allen, A. Ingargiola, LMFIT: Non-linear least-square minimization and curve-fitting for Python, Zenodo (2014); https://doi.org/10.5281/zenodo.11813.
41. P. Virtanen, R. Gommers, T. E. Oliphant, M. Haberland, T. Reddy, D. Cournapeau, E. Burovski, P. Peterson, W. Weckesser, J. Bright, S. J. van der Walt, M. Brett, J. Wilson, K. J. Millman, N. Mayorov, A. R. J. Nelson, E. Jones, R. Kern, E. Larson, C. J. Carey, İ. Polat, Y. Feng, E. W. Moore, J. VanderPlas, SciPy 1.0 Contributors, SciPy 1.0: Fundamental algorithms for scientific computing in Python. *Nat. Methods* **17**, 261–272 (2020). doi:10.1038/s41592-019-0686-2 Medline
42. J. Razzell Hollis, D. Rheingold, R. Bhartia, L. W. Beegle, An optical model for quantitative Raman microspectroscopy. *Appl. Spectrosc.* **74**, 684–700 (2020). doi:10.1177/0003702819895299 Medline
43. B. L. Carrier, W. J. Abbey, L. W. Beegle, R. Bhartia, Y. Liu, Attenuation of ultraviolet radiation in rocks and minerals: Implications for Mars science. *J. Geophys. Res. Planets* **124**, 2599–2612 (2019). doi:10.1029/2018JE005758
44. K. E. Kuebler, B. L. Jolliff, A. Wang, L. A. Haskin, Extracting olivine (Fo–Fa) compositions from Raman spectral peak positions. *Geochim. Cosmochim. Acta* **70**, 6201–6222 (2006). doi:10.1016/j.gca.2006.07.035
45. M. Veneranda, J. A. Manrique-Martinez, G. Lopez-Reyes, J. Medina, I. Torre-Fdez, K. Castro, J. M. Madariaga, C. Lantz, F. Poulet, A. M. Krzesińska, H. Hellevang, S. C. Werner, F. Rull, Spectroscopic study of olivine-bearing rocks and its relevance to the ExoMars rover mission. *Spectrochim. Acta A Mol. Biomol. Spectrosc.* **223**, 117360 (2019). doi:10.1016/j.saa.2019.117360 Medline
46. K. S. Edgett, Perseverance's SHERLOC WATSON – post-landing refinement of relations between focus, range, and image scale using images acquired on Mars, plus an update on particulates on the detector, Zenodo (2021); https://doi.org/10.5281/zenodo.5555292.
47. S. Leutenegger, M. Chili, R. Y. Siegwart, "BRISK: Binary Robust invariant scalable keypoints" in *2011 International Conference on Computer Vision* (IEEE, 2011), pp. 2548–2555.
48. G. Bradski, The OpenCV Library. *Dr. Dobb's J.* **120**, 122–125 (2000).
49. Z. Wu, A. Wang, Z. Ling, Spectroscopic study of perchlorates and other oxygen chlorides in a Martian environmental chamber. *Earth Planet. Sci. Lett.* **452**, 123–132 (2016). doi:10.1016/j.epsl.2016.07.044
50. J. D. Stopar, P. G. Lucey, S. K. Sharma, A. K. Misra, G. J. Taylor, H. W. Hubble, Raman efficiencies of natural rocks and minerals: Performance of a remote Raman system for planetary exploration at a distance of 10 meters. *Spectrochim. Acta A Mol. Biomol. Spectrosc.* **61**, 2315–2323 (2005). doi:10.1016/j.saa.2005.02.030 Medline
51. M. R. Salvatore, T. A. Goudge, M. S. Bramble, C. S. Edwards, J. L. Bandfield, E. S. Amador, J. F. Mustard, P. R. Christensen, Bulk mineralogy of the NE Syrtis and Jezero crater regions of Mars derived through thermal infrared spectral analyses. *Icarus* **301**, 76–96 (2018). doi:10.1016/j.icarus.2017.09.019
52. R. J. Smith, S. M. McLennan, C. N. Achilles, E. Dehouck, B. H. N. Horgan, N. Mangold, E. B. Rampe, M. Salvatore, K. L. Siebach, V. Sun, X-ray amorphous components in sedimentary rocks of Gale Crater, Mars: Evidence for ancient formation and long-lived aqueous activity. *J. Geophys. Res. Planets* **126**, e2020JE006782 (2021). doi:10.1029/2020JE006782
53. E. Eshelman, M. G. Daly, G. Slater, E. Cloutis, Time-resolved detection of aromatic compounds on planetary surfaces by ultraviolet laser induced fluorescence and Raman spectroscopy. *Planet. Space Sci.* **119**, 200–207 (2015). doi:10.1016/j.pss.2015.09.021
54. E. Eshelman, M. G. Daly, G. Slater, E. Cloutis, Detecting aromatic compounds on planetary surfaces using ultraviolet time-resolved fluorescence spectroscopy. *Planet. Space Sci.* **151**, 1–10 (2018). doi:10.1016/j.pss.2017.09.003
55. E. A. Lalla, M. Konstantinidis, E. Lymer, C. M. Gilmour, J. Freemantle, P. Such, K. Cote, G. Groemer, J. Martinez-Frias, E. A. Cloutis, M. G. Daly, Combined spectroscopic analysis of terrestrial analogs from a simulated astronaut mission using the laser-induced breakdown spectroscopy (LIBS) Raman sensor: Implications for Mars. *Appl. Spectrosc.* **75**, 1093–1113 (2021). doi:10.1177/00037028211016892 Medline
56. S. Shkolyar, E. J. Eshelman, J. D. Farmer, D. Hamilton, M. G. Daly, C. Youngbull, Detecting kerogen as a biosignature using colocated UV time-gated Raman and fluorescence spectroscopy. *Astrobiology* **18**, 431–453 (2018). doi:10.1089/ast.2017.1716 Medline
57. S. Shkolyar, E. Lalla, M. Konstantindis, K. Cote, M. G. Daly, A. Steele, Detecting Ce^{3+} as a biosignature mimicker using UV time-resolved laser-induced fluorescence and Raman spectroscopy: Implications for planetary missions. *Icarus* **354**, 114093 (2021). doi:10.1016/j.icarus.2020.114093
58. M. Gaft, R. Reisfeld, G. Panczer, *Modern Luminescence Spectroscopy of Minerals and Materials* (Springer, 2015).
59. M. R. Baril, D. J. Huntley, Optal excitation spectra of trapped electrons in irradiated feldspars. *J. Phys. Condens. Matter* **15**, 8011–8027 (2003). doi:10.1088/0953-8984/15/46/017
60. K. Sudarsanan, R. A. Young, Significant precision in crystal structural details - Holly Springs hydroxyapatite. *Acta Crystallogr. B* **B25**, 1534–1543 (1969). doi:10.1107/S0567740869004298
61. D. J. Lieftink, T. G. Nijland, C. Maijer, The behavior of rare-earth elements in high-temperature Cl-bearing aqueous fluids; results from the Odegardens-Verk natural laboratory. *Can. Mineral.* **34**, 149–158 (1994).
62. F. M. McCubbin, E. H. Hauri, S. M. Elardo, K. E. Vander Kaaden, J. Wang, C. K. Shearer Jr., Hydrous melting of the martian mantle produced both depleted and enriched shergottites. *Geology* **40**, 683–686 (2012). doi:10.1130/G33242.1
63. S. L. Nadeau, S. Epstein, E. Stolper, Hydrogen and carbon abundances and isotopic ratios in apatite from alkaline intrusive complexes, with a focus on carbonatites. *Geochim. Cosmochim. Acta* **63**, 1837–1851 (1999). doi:10.1016/S0016-7037(99)00057-5
64. R. Bhartia, W. Hug, R. Reid, L. Beegle, "Explosives detection and analysis by fusing deep ultraviolet native fluorescence and resonance Raman spectroscopy" in *Laser-Based Optical Detection of Explosives*, P. M. Pellegrino, E. L. Holthoff, M. E. Farrell, Eds. (Taylor & Francis Group, 2015), pp. 67–97.
65. M. Suto, X. Wang, J. Shan, L. C. Lee, Quantitative photoabsorption and fluorescence spectroscopy of benzene, naphthalene, and some derivatives at 106–295 nm. *J. Quant. Spectrosc. Radiat. Transf.* **48**, 79–89 (1992). doi:10.1016/0022-4073(92)90008-R

ACKNOWLEDGMENTS

We thank the entire Perseverance rover team. The work described in this paper was partially carried out at the Jet Propulsion Laboratory, California Institute of Technology, under a contract with the National Aeronautics and Space Administration. We extend special thanks to K. Edgett for his team contributions and thank S. Le Mouélic helpful comments. We thank V. Chevrier and two anonymous reviewers for their improvements to the manuscript. **Funding:** E.L.S. was supported by a NASA Earth and Space Science Fellowship (NESSF) (grant 80NSSC18K1255). J.R.H. and A.C.F. were supported by a NASA Postdoctoral Program fellowship. E.L.S. J.R.H., A.S., L.W.B., R.B., B.L.E., P.G.C., M.F., F.M.M., and A.S.B. were supported by the NASA Mars 2020 Phase-E funds to the SHERLOC investigation. A.J.W. was supported by the NASA M2020 Participating Scientist Program. T.F. was supported by an Italian Space Agency grant (#2017-48-H.0). A.G.F was supported by the European Research Council Consolidator Grant (#818602). R.W. was funded by NASA contracts NNH15AZ25I and NNH13ZDA018O. S.S. was supported by the Swedish National Space Agency (contracts 137/19 and 2021-00092). K. H.-L. is funded by an Aurora Research

Fellowship from the UK Space Agency (grant ST/V00560X/1). **Author contributions:** E.L.S. and J.R.H. contributed equally to data analysis. E.L.S. and J.R.H. wrote the manuscript with substantial contributions from A.S. and E.C. L.W.B. and R.B. are the principal and deputy investigators of the SHERLOC instrument. K.U. developed the Loupe software. P.C., S.S., B.L.E., W.J.A., S.A.A, E.L.B., B.L.B., A.S.B., S.V.B., L.D., D.M.F., T.F., A.C.F., M.F., K.H.-L., W.F.H., J.E.H., S.I., R.S.J., M.R.K., C.L., F.M.M., B.E.N., C.R.S.-V., R.D.R., S.S., S.S., K.S., A.W., K.H.W., K.W., B.W., A.Y., and R.Y. are members of the SHERLOC science and operations teams, who participated in planning and carrying out SHERLOC data acquisitions, calibration, and processing during rover operations. The SHERLOC science team also provided laboratory measurements, data analysis, and contributed to writing of the initial manuscript. T.K., K.R.M., and Y.L. are members of the PIXL team, who assisted in paired SHERLOC and PIXL data analysis. K.C.B., O.B., T.B., A.J.B., E.C., A.G.F., K.A.F., L.C.K., P.K., L.M., J.I.N., M.S., M.A.S., S.K.S., D.L.S., J.I.S., R.J.S., B.P.W., A.J.W., R.C.W., and M.P.-Z. are members of the wider Perseverance rover science team; they contributed to planning the SHERLOC data acquisitions, participated in data interpretation, and/or assisted in revising the manuscript. **Competing interests:** We declare no competing interests. **Data and materials availability:** The data are available on the Planetary Data System, in the bundles for SHERLOC and WATSON (*31*), Mastcam-Z (*32*), NavCam and Hazcam (*33*), PIXL (*34*), and Supercam (*35*); the exact files we used are listed in the supplementary material. The Loupe software is archived on Zenodo (*36*). Laboratory data used for the study are archived at Zenodo (*37*).

SUPPLEMENTARY MATERIALS

science.org/doi/10.1126/science.abo5204
Materials and Methods
Figs. S1 to S23
Table S1
References (*38*–*65*)

Submitted 15 February 2022; accepted 10 November 2022
Published online 23 November 2022
10.1126/science.abo5204

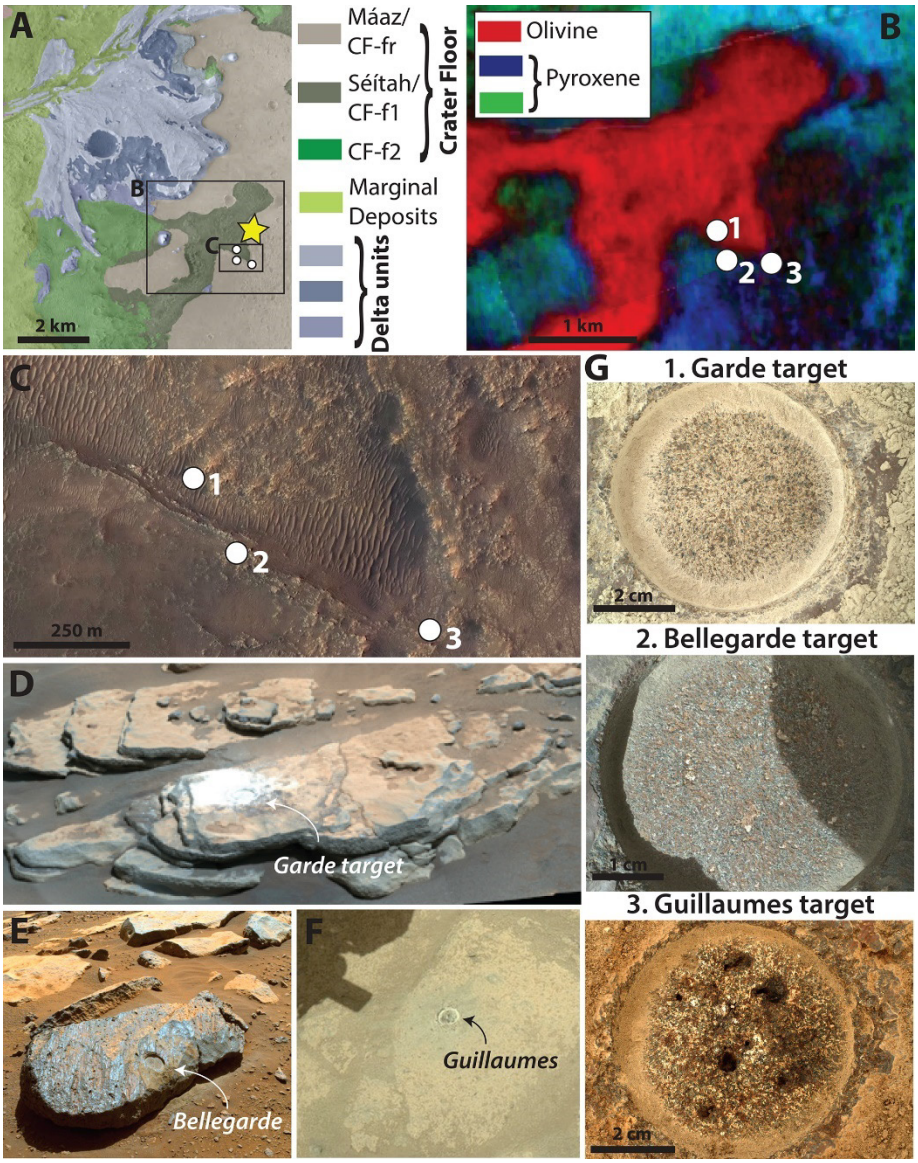

Fig. 1. Rover images of the three abraded targets and their orbital context. (**A**) Map of orbitally defined geological units within Jezero crater (*12*), including the Crater Floor Fractured Rough unit (CF-fr) equivalent to the Máaz Fm and the Crater Floor Fractured 1 (CF-f1) unit equivalent to the Séítah Fm. Star shows the landing site, while white circles show the position of the three abraded targets. The locations of (B) and (C) are outlined in black rectangles. [Adapted by permission from Springer Nature Customer Service Center GmbH, Springer Nature *Space Sci. Rev.* (*12*), copyright (2020)] (**B**) Orbital infrared spectroscopy map showing the location of pyroxene- or olivine-bearing materials in the study area from (*4*). Labels on white circles correspond to (G). (**C**) HiRISE view of study area (*30*). (**D**) Mastcam-Z image showing the Garde patch on the Bastide outcrop. (**E**) Hazcam image showing the Bellegarde patch on the Rochette rock. (**F**) Navcam image showing the Guillaumes patch on the Roubion outcrop. (**G**) WATSON images of abraded targets analyzed in this study. Greyscale images are available in figs. S9 to S11.

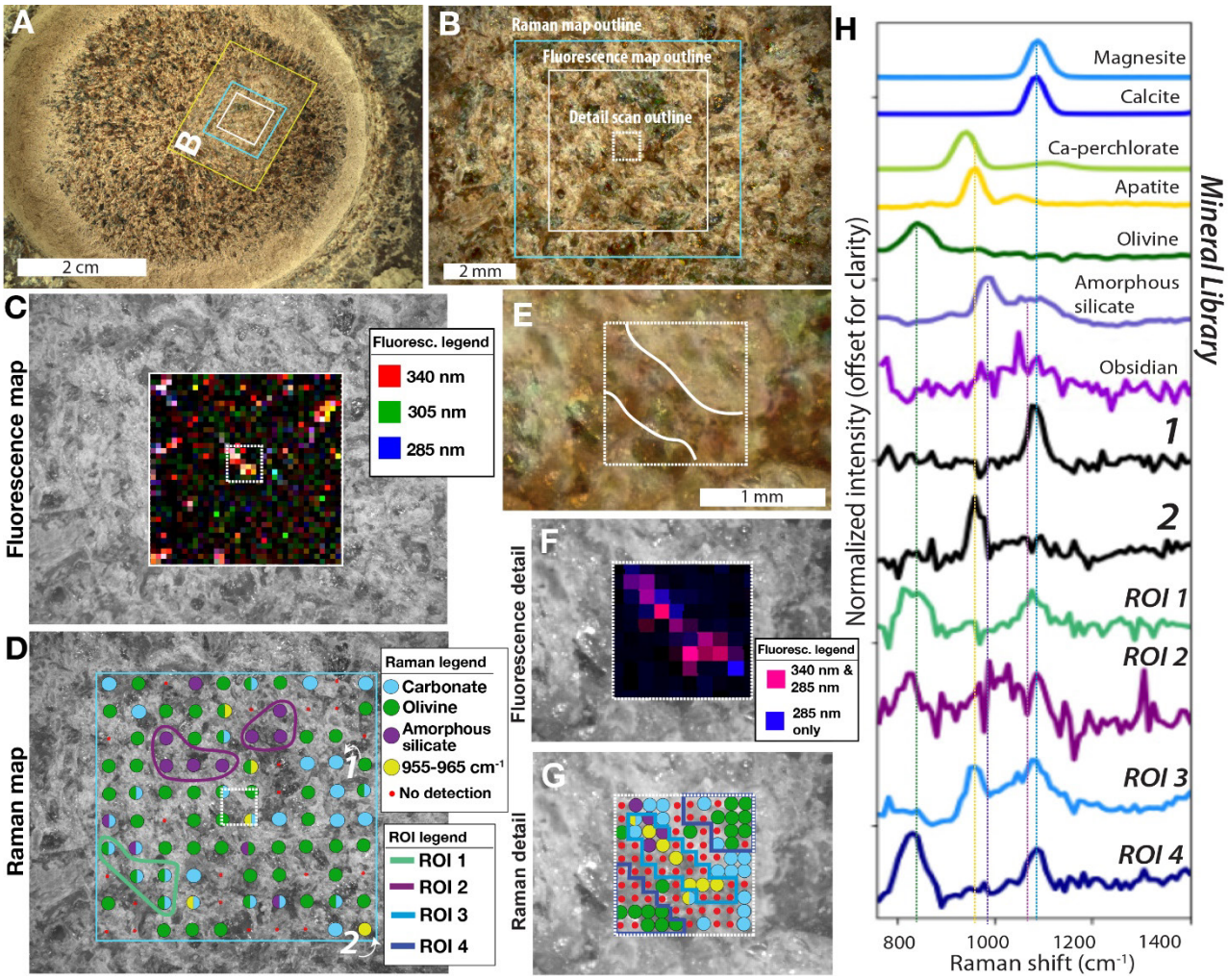

Fig. 2. SHERLOC Raman and fluorescence results for the Garde abraded patch. (**A**) WATSON image. (**B**) Context image and scan outlines. (**C** to **G**) Greyscale version of context image with data superimposed. (C) Fluorescence map showing the intensity of three main features centralized at 340 nm, 305 nm, and 285 nm in red, green, and blue respectively. (D) Raman mineral maps showing the location of detected olivine, carbonate, phosphate, and weak amorphous silicate features. Purple and green outlines indicate regions of interest (ROIs 1-2, numbered in white) were used for spectra shown in (H). (E) Zoom in on (B) shows fluorescence correlation with intergranular spaces (outlined in white lines). (F) Fluorescence map from detail scan. (G) Raman map from detail scan and ROI 3-4 outlines intergranular and mineral domain textures [same legend as in (D)] used in (H). (**H**) Average ROI and single point (1-2) SHERLOC spectra [positions in (D) and (G)] compared with laboratory measurements. Greyscale images are available in figs. S12 to S15.

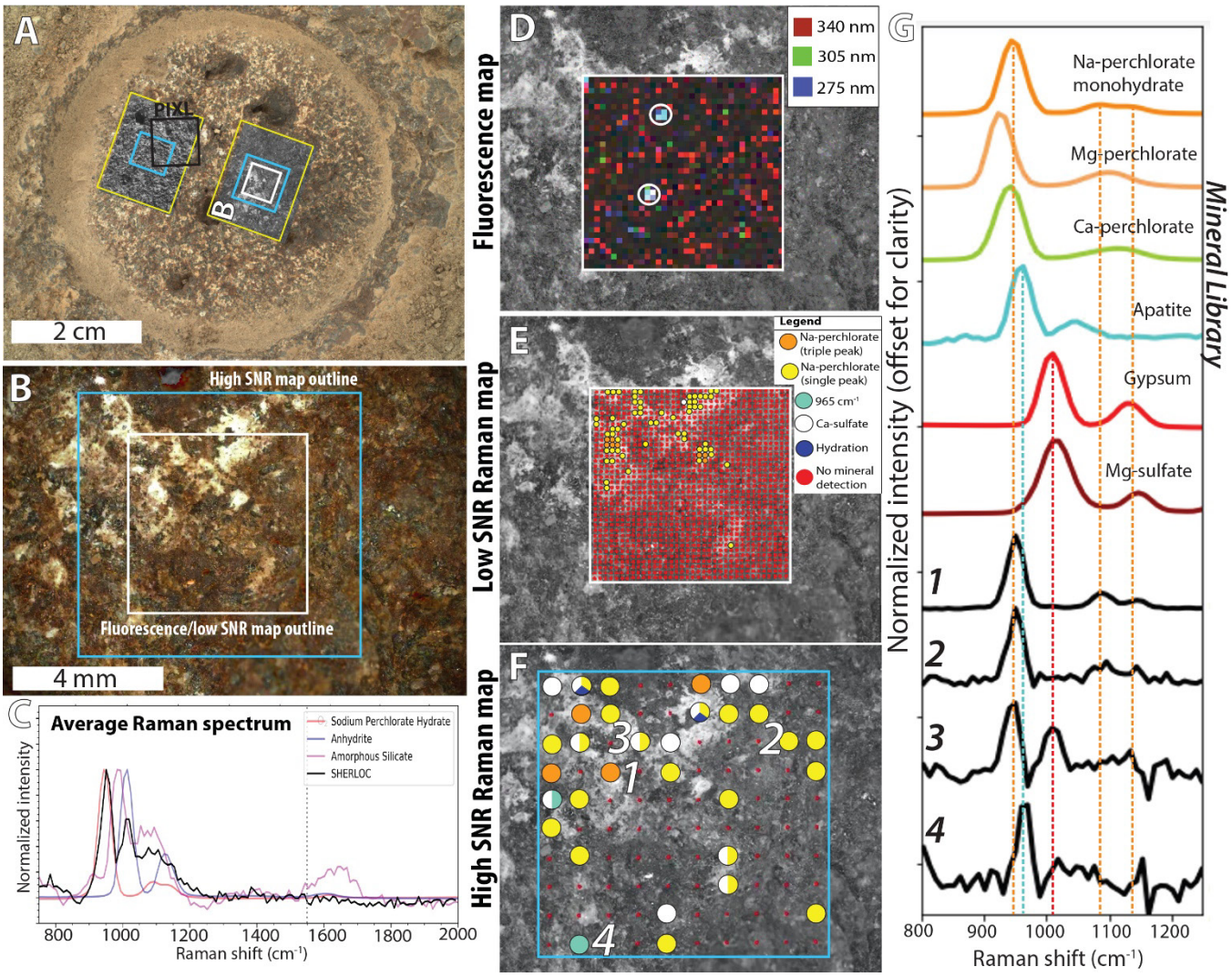

Fig. 3. SHERLOC Raman and fluorescence results for the Guillaumes abraded patch. (**A**) WATSON image. Two SHERLOC scans (yellow outlines) and one PIXL scan (black outline) shown. (**B**) Context image and scan outlines. (**C**) Average Raman spectrum compared with laboratory measurements of amorphous silicate, Na-perchlorate, and anhydrite. Laboratory spectral features at 1500-1600 cm^{-1} are O_2 (vertical, dotted line) and organic contaminants. (**D** to **F**) Greyscale version of context image with data superimposed. (D) Fluorescence map showing the intensity of three main features centralized at 340 nm, 305 nm, and 275 nm in red, green, and blue respectively. White circles indicate locations exposed to SuperCam laser shots (*8*). (E and F) Low and high signal-to-noise ratio (SNR) (*8*) Raman mineral maps showing the locations of detected perchlorate, Ca-sulfate with and without hydration, and 965 cm^{-1} peaks. (**G**) Raman spectra [positions indicated with numbers in (E) and (F)] from SHERLOC (1-4) compared with laboratory measurements. Greyscale images are available in figs. S16 to S19.

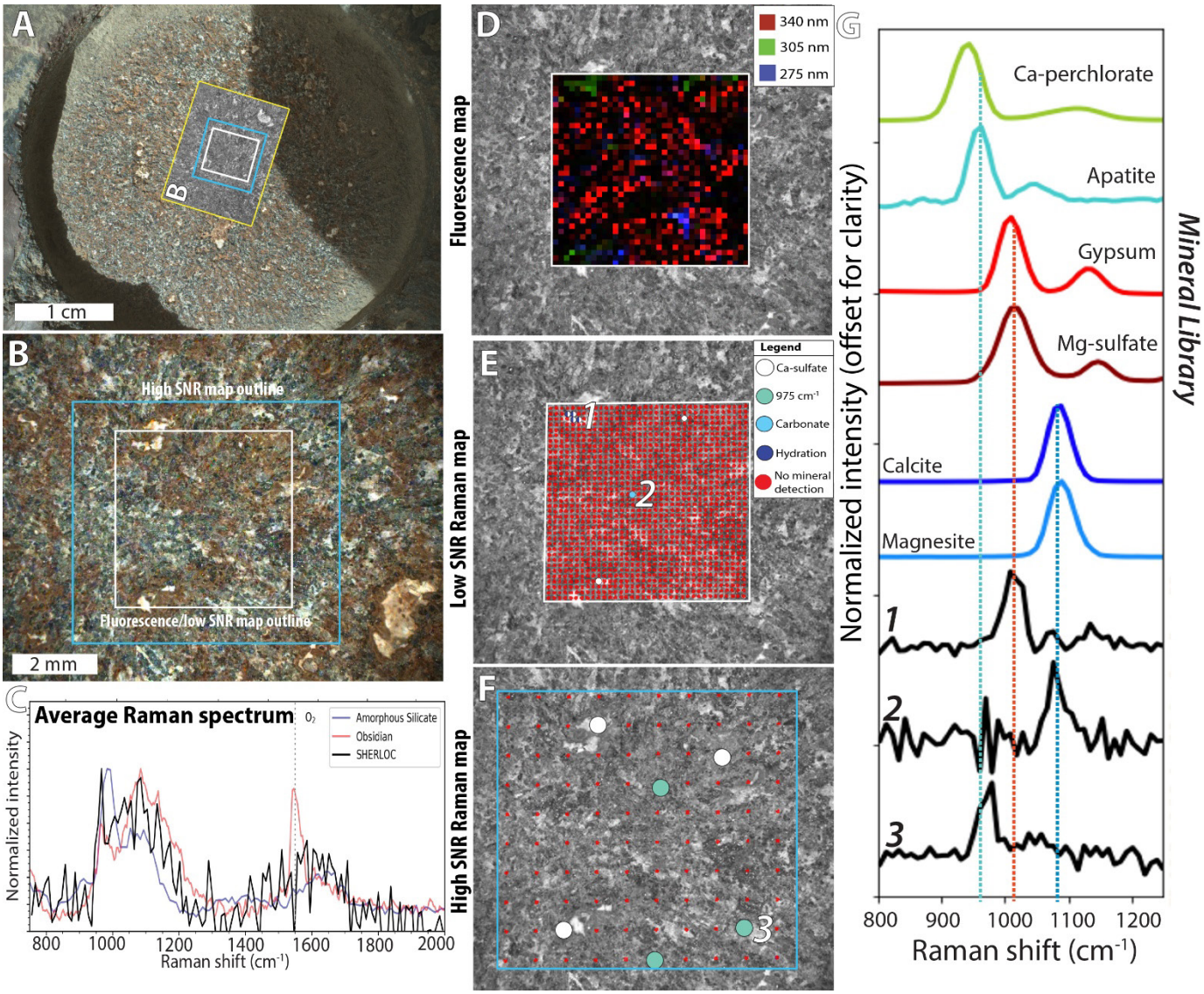

Fig. 4. SHERLOC Raman and fluorescence results for the Bellegarde abraded patch. (**A**) WATSON image. (**B**) Context image and scan outlines. (**C**) Average Raman spectrum compared with laboratory measurements of amorphous silicate and obsidian. Laboratory spectral features at 1500-1600 cm^{-1} are O_2 (vertical, dotted line) and trace organic contaminants. (**D** to **F**) Greyscale version of context image with data superimposed. (D) Fluorescence map showing the intensity of three main features centralized at 340 nm, 305 nm, and 275 nm in red, green, and blue respectively. (E and F) Low and high signal-to-noise ratio (SNR) (*8*) Raman mineral maps showing the location of detected Ca-sulfate with and without hydration, carbonate, and 975 cm^{-1} peaks. (**G**) Raman spectra [positions indicated with numbers in (E) and (F)] from SHERLOC (1-3) compared with laboratory measurements [full hydrated sulfate spectrum in fig. S3 (*8*)]. Greyscale images are available in figs. S20 to S23.

Science

Aqueous alteration processes in Jezero crater, Mars-implications for organic geochemistry

Eva L. SchellerJoseph Razzell HollisEmily L. CardarelliAndrew SteeleLuther W. BeegleRohit BhartiaPamela ConradKyle UckertSunanda SharmaBethany L. EhlmannWilliam J. AbbeySanford A. AsherKathleen C. BenisonEve L. BergerOlivier BeyssacBenjamin L. BleefeldTanja BosakAdrian J. BrownAaron S. BurtonSergei V. BykovEd CloutisAlberto G. FairénLauren DeFloresKenneth A. FarleyDeidra M. FeyTeresa FornaroAllison C. FoxMarc FriesKeyron Hickman-LewisWilliam F. HugJoshua E. HuggettSamara ImbeahRyan S. JakubekLinda C. KahPeter KelemenMegan R. KennedyTanya KizovskiCarina LeeYang LiuLucia MandonFrancis M. McCubbinKelsey R. MooreBrian E. NixonJorge I. NúñezCarolina Rodriguez Sanchez-VahamondeRyan D. RoppelMitchell SchulteMark A. SephtonShiv K. SharmaSandra SiljeströmSvetlana ShkolyarDavid L. ShusterJustin I. SimonRebecca J. SmithKathryn M. StackKim SteadmanBenjamin P. WeissAlyssa WerynskiAmy J. WilliamsRoger C. WiensKenneth H. WillifordKathrine WinchellBrittan WogslandAnastasia YanchilinaRachel YinglingMaria-Paz Zorzano

Science, **Ahead of Print** • DOI: 10.1126/science.abo5204